JOURNAL OF SPACECRAFT AND ROCKETS
Vol. 34, No. 6, November–December 1997

Hypersonic Thermal Environment of a Proposed Single-Stage-to-Orbit Vehicle

K. James Weilmuenster,* P. A. Gnoffo,* F. A. Greene,† C. J. Riley,‡ and H. H. Hamilton II*
NASA Langley Research Center, Hampton, Virginia 23681

The thermal environment of a representative single-stage-to-orbit winged body vehicle has been investigated at a Mach number of 21.89 and an altitude of 233,000 ft, which corresponds to the peak heating condition on a nominal re-entry trajectory. Both surface heating and temperatures are mapped for the baseline configuration and for control surfaces both fixed (tip fins) and deflected (body flap and elevons). The thermal environment is predicted for angles of attack of 28, 32, and 36 deg; for body flap deflections of 10 and 20 deg; and for a matrix of tip fin parameters based on leading-edge radius and leading-edge sweep angle. The analysis is based on laminar flow in chemical equilibrium and chemical nonequilibrium including catalytic surface effects. The analysis shows that, in the vicinity of the wing fuselage juncture and tip fin leading edge, the localized heating can be as much as three times and temperatures as much as one-third greater than those found at the stagnation point. These extremes are the result of shock interactions that are influenced by vehicle aerolines and attitude, as well as the chemical state of the gas in the flowfield.

Nomenclature

d	= deflection angle, deg
h	= altitude, ft
M	= Mach number
Q	= surface heat flux, Btu/ft^2-s
Re	= unit Reynolds numbers per foot
r	= radius, in.
T	= temperature, °F
x, y, z	= Cartesian coordinates, local coordinate system, in.
α	= angle of attack, deg
Λ	= tip fin sweep angle, deg

Subscripts

cs	= control surface
le	= leading edge
w	= wall
∞	= freestream

Introduction

NASA is laying the groundwork for the next-generation space transportation system that is envisioned as a family of fully reusable, robust vehicles that operate much like aircraft for commercial airlines. A foundation for this new space transportation system was established by a NASA, Department of Defense, Department of Transportation interagency study.[1] This study examined a wide spectrum of space transportation system concepts and concluded that the single-stage-to-orbit (SSTO) rocket-powered vehicle was the most viable technological approach to achieve an order of magnitude reduction in the life cycle cost (compared to the Space Shuttle Orbiter) by the year 2008.

The former Space Systems Division at the NASA Langley Research Center performed systems analysis studies and generated aerodynamic and aeroheating information via computational fluid dynamics (CFD) and ground-based testing for a number of space transportation system concepts. Included in these studies was a SSTO, vertical takeoff/horizontal landing winged body concept proposed as a candidate advanced manned launch system (AMLS).[2] Results for this AMLS concept were introduced into the Access to Space Study.[1] Because of the advantages provided by this concept, a substantial effort was undertaken to fully assess and to optimize the aerodynamic performance across the speed regime for entry to landing and to determine aeroheating characteristics for design of the thermal protection system (TPS).

The authors have shown that CFD can provide an accurate prediction of vehicle surface heating and temperature for hypersonic, laminar flow over the Shuttle Orbiter vehicle through the proper modeling of the reacting gas chemistry in the flowfield, as well as the interaction of the surface composition with that flowfield.[3] In addition to properly modeling the vehicle's environment, a CFD analysis is particularly helpful when predicting surface properties in localized surface areas of topological complexity or areas affected by shock interactions.

Historically, the Shuttle Orbiter has operated within the limits of its TPS. However, to meet the operational goals of an advanced launch system, new approaches to vehicle construction and thermal protection will have to be utilized; the optimization of these new approaches will require a thorough knowledge of the thermal environment of the vehicle. In addition, this new class of vehicle can be more or less geometrically complex than the Shuttle Orbiter and, if more complex, such as the one addressed in this paper, may see surface temperatures higher than those experienced by the Orbiter. In this paper, the CFD techniques[3] will be used to define the thermal environment of a proposed SSTO vehicle at peak heating on the entry trajectory. Results will be presented for multiple angles of attack, for different control surface geometries (both movable and fixed) and for chemical equilibrium and nonequilibrium flow.

Geometry and Grids

The coordinate system in which the geometries are described is shown in Fig. 1. The full vehicle geometry is shown in Fig. 2 with the movable control surfaces (elevons and body flap) deflected 20 deg. The surface was constructed in the PRO ENGINEERING solid modeling software and transferred through a standard IGES format to the ICEM surface modeling system, which was used to generate a 161 × 129 surface grid. The volume grids were created using the GRIDGEN software[4] to define the volume outer boundary and the 3DMAGGS code[5] to define the internal volume grid that has 65 points between the wall and the outer boundary. To obtain a quality Navier–Stokes solution, it is necessary to maintain grid orthogonality at the surface of the vehicle. For this study, a great

Received May 6, 1996; revision received June 15, 1997; accepted for publication July 19, 1997.

*Senior Research Engineer, Aerothermodynamics Branch, Research Technology Group. Associate Fellow AIAA.

†Research Engineer, Aerothermodynamics Branch, Research Technology Group.

‡Research Engineer, Aerothermodynamics Branch, Research Technology Group. Member AIAA.

Table 1 Computational point

Time, s	Altitude, ft	Density, kg/m^3	Temperature, K	Velocity, m/s	α, deg	Mach no.	Re/ft
1,032	233,000	0.0000717	217.0	6,461	32.00	21.9	5.55×10^4

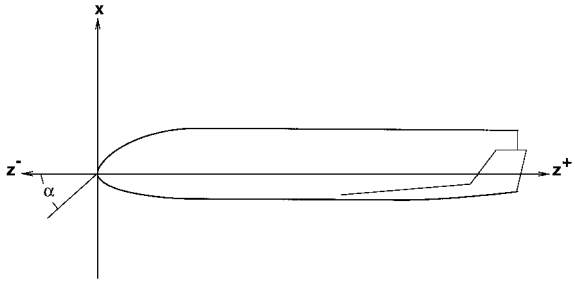

Fig. 1 Vehicle orientation in the LAURA coordinate system.

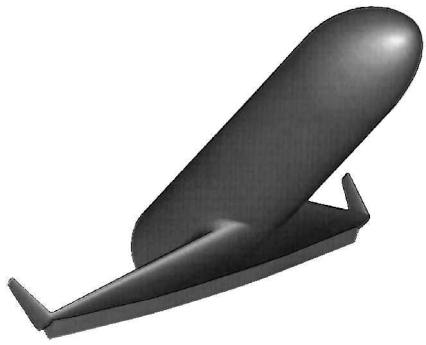

Fig. 2 Baseline SSTO vehicle surface definition with control surfaces deflected.

deal of care was taken to ensure that the grid was normal to the surface at all points on the body.

The normal grid density chosen for this study is based on the extensive Shuttle Orbiter calculations,[3,6] which included grid resolution studies as well as comparisons with experimental and flight data. These studies showed that, whereas surface pressure is relatively insensitive to grid quality, computed surface heat flux is sensitive to not only grid density but also grid distribution (stretching) and cell Reynolds number at the wall. This work also showed that, when the grid is properly distributed, 64 nodes between the body and the outer boundary is sufficient for the Mach and Reynolds numbers being considered here, to compute accurate surface heat flux. Because the vehicle of interest is operating in an environment similar in angle of attack and freestream conditions to the Orbiter, the authors feel the grid density and topology used herein is adequate to predict the thermal environment of this vehicle.

The vehicle considered is 2227 in. in length with a wing semispan of 570 in. It is a circular body set on a 45-deg swept wing based on a NACA 0012 airfoil section with a leading-edge radius of 11 in. at the wing root and 2.5 in. at the wing tip. The wing tip fin controller shown in Fig. 2 represents the baseline configuration for this part of the vehicle geometry and is based on a NACA 0012 airfoil section with a 1.74-in. leading-edge radius at the half-span and is swept 32 deg relative to the vertical.

Several other tip fin configurations were devised for this study. In addition to the baseline geometry, two other 1.74-in. leading-edge radius fins with leading-edge sweep angles of 24 and 40 deg were constructed. The $\Lambda = 40$-deg configuration is shown in Fig. 3. The trailing edge of the fins for the $\Lambda = 24$ and 40 deg cases were swept to conform to the systems study requirement that the height and platform area of the fins were to remain constant. Also, tip fins with leading-edge radii of 1.16 and 2.31 in. at the semispan point and a $\Lambda = 32$ deg were constructed for use in this study.

Computational Techniques: Flowfield Solutions

Code

The LAURA code[7–9] can compute inviscid or viscous solutions for perfect gas flows and reacting gas flows in either an equilibrium or a nonequilibrium state. The inviscid flux is constructed using Roe's[10] flux-difference splitting and Harten's[11] entropy fix with second order corrections based on Yee's symmetric total variation diminishing scheme.[12]

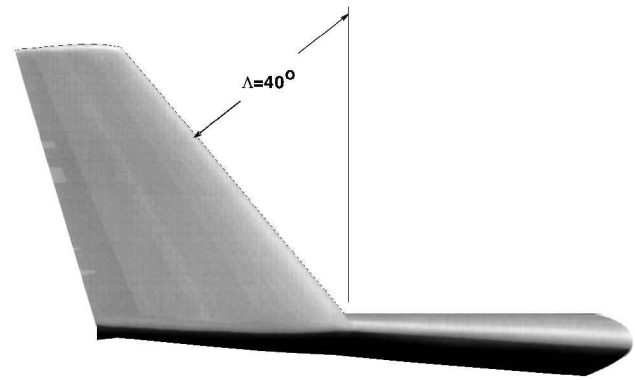

Fig. 3 Representative tip fin geometry, Λ = 40 deg.

Chemistry

Tannehill's[13] curve fits are used for the thermodynamic and transport properties of equilibrium air. A seven-species chemical reaction model[3] is used for the reacting gas computations. The species N, O, N_2, O_2, NO, NO^+, and $\bar{e}$ are included in the model.

Boundary Conditions

The usual no-slip condition is imposed at the wall for the viscous computations. The surface temperature is based on a radiative equilibrium wall boundary condition.[3] Freestream conditions are set at points on the outer boundary of the computational domain; the exit plane is set such that the inviscid outflow is supersonic.

Thermal Surface Model

For this analysis, the TPS for the vehicle is assumed to be a material of low catalyticity similar to that used on the Shuttle Orbiter. Application of the catalytic wall boundary condition is based on the work of Thompson.[14] This approach has been shown to produce results that are in good agreement with Orbiter flight data.[3,14]

Solution Technique/Strategy

A multiblock solution strategy is applied in two stages. The first stage may be regarded as a space marching solution, like the parabolized Navier–Stokes methods, except that three-dimensional data blocks are employed rather than two-dimensional data planes. The second stage is a conventional, global relaxation, which uses the first-stage solution as an initial condition. The advantages of the three-dimensional block marching over two-dimensional block marching are that solution robustness is not sacrificed when employing second-order discretization in the streamwise direction and embedded subsonic pockets and shock/boundary-layer interactions are easily computed, provided that the outflow boundary of the subdomain is intelligently chosen. The subdomain boundaries are easily tailored to the physics of a given application. A detailed description of this solution technique can be found in Ref. 3.

Solutions for multiple tip fin and control surface configurations are based on solutions for the baseline configuration at a given angle of attack. For the tip fins, the computational subdomain was bounded by an upstream plane and wind and leeside planes from the baseline solution.

Results

All of the calculations are based on the freestream conditions given in Table 1. These conditions correspond to the peak,

Table 2 TPS material thermal limits[15]

Material	Maximum temperature, °F	
	Multiple use	Single use
Blankets		
FRSI	700	800
PBI	700/900	1100
AFRSI	1200	2000
TABI	2000	2200
Rigid ceramics		
LI-900	2500	2700
LI-2200	2600	2800
FRCI-12	2600	2800
AETB-12/TUFI	2500	2700
AETB/RCG	2600	2800
ASMI	2600	2900
AETB-8/RCG	2600	2800
Metal		
Titanium	1000	
Rene 41	1600	
Inconel 617	1800	2000
RCC/ACC		
Short-term use	3000	3300
Extended use	2600/2800	

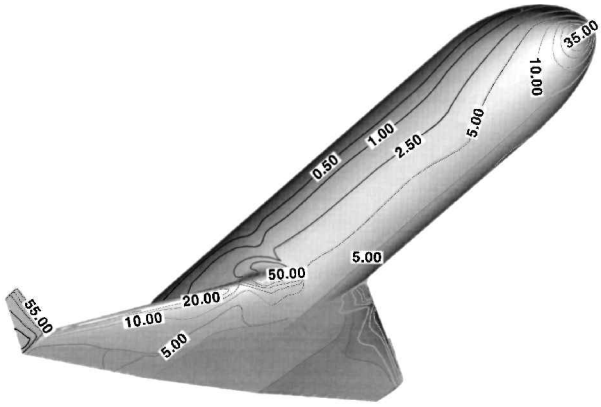

a) Equilibrium

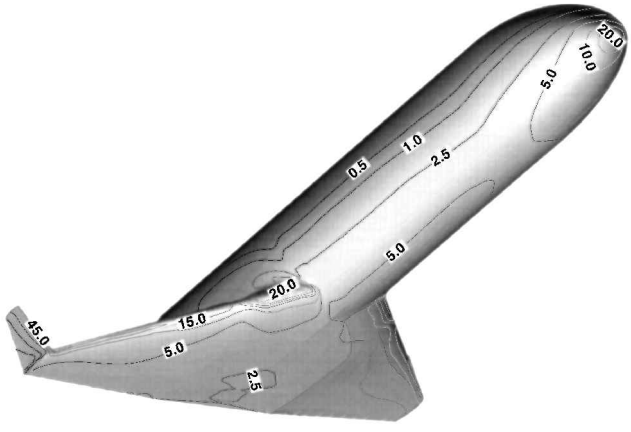

b) Nonequilibrium

Fig. 4 Surface heat flux map of the baseline configuration at 32-deg angle of attack for both equilibrium and nonequilibrium flow chemistry (Btu/ft^2-s).

stagnation-point heating on a SSTO vehicle nominal entry trajectory. For reference purposes, the multiple-use and single-use temperature limits[15] for some representative traditional and nontraditional TPS materials are given in Table 2.

Baseline Configuration

Surface heating and temperature contour plots for equilibrium and nonequilibrium flow for the baseline configuration are shown in Figs. 4a, 4b, 5a, and 5b, where the viewing angle has been chosen to emphasize the wind surface of the vehicle. The equilibrium solution represents a very good approximation to a nonequilibrium

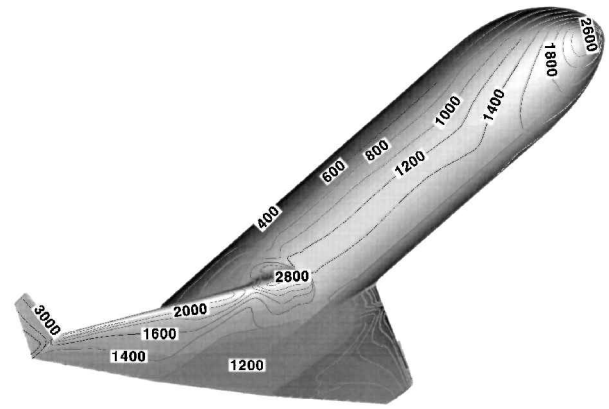

a) Equilibrium

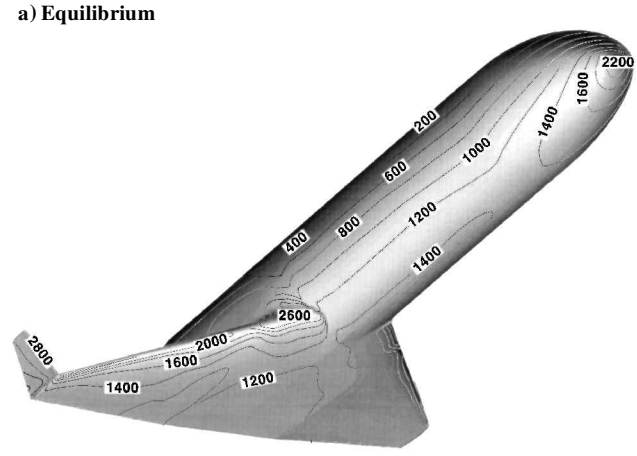

b) Nonequilibrium

Fig. 5 Surface temperature map of the baseline configuration at 32-deg angle of attack for both equilibrium and nonequilibrium flow chemistry (°F).

solution based on a fully catalytic wall boundary condition and is computationally more efficient than the nonequilibrium calculation. The nonequilibrium solution provides an indication of the effect of finite wall catalyticity and is based on the surface properties of Shuttle Orbiter tiles. Over the vast majority of the vehicle, the surface heating and temperature are on the order of 10 Btu/ft^2-s and 1500°F regardless of the flow chemistry model being used. Thus, for most of the vehicle surface, the TPS requirements can be met by a combination of the thermal blanket and rigid tile materials (Table 2). These plots also show four areas of higher heating: 1) the forebody stagnation point, 2) the wing/fuselage juncture, 3) the wing leading edge, and 4) the tip fin leading edge. For both the equilibrium and nonequilibrium flows, the thermal maximums occur on the tip fin leading edge. On the windward surface, as expected, the equilibrium flow model produces generally higher thermal levels over the entire vehicle. In the following discussion, the four areas of higher heating just identified will be examined in more detail.

The predicted surface thermal environment in the upper and lower symmetry planes is shown in Figs. 6a and 6b as a function of vehicle axial length. In the upper symmetry plane, out of the immediate stagnation region, the heating is negligible and the surface temperature is near the freestream value. In the lower symmetry plane, the effect of chemistry model on the surface thermal environment comes into play, particularly in the stagnation region. At the stagnation point, a change from a nonequilibrium to an equilibrium chemistry model results in an 80% increase in surface heat flux. Downstream of the immediate stagnation region, the differential in surface heat flux is 20–30% over the remaining length of the vehicle. Referring to Table 2, the resulting surface temperatures in the stagnation region are well within the multiuse limits of reenforced carbon carbon (RCC)/advanced carbon carbon (ACC), although the equilibrium temperatures are approaching the extended-use limit of these materials typically used in the construction of vehicle nosecap TPS.

Similar plots of the predicted surface thermal environment at the wing/fuselage juncture and along the wing leading edge are shown

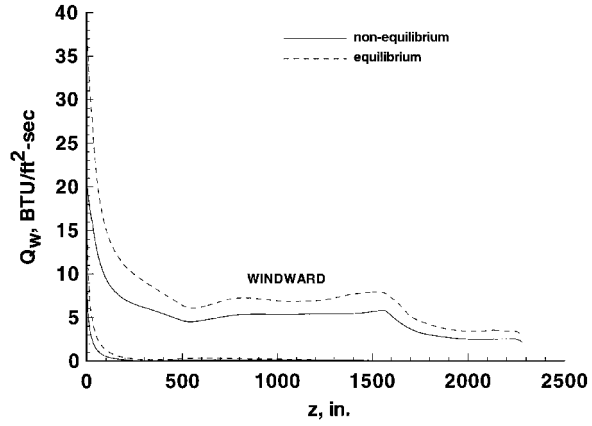

a) Heat flux

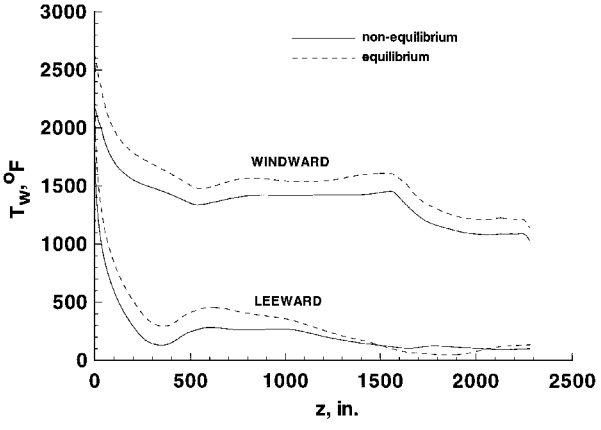

b) Temperature

Fig. 6 Windward and leeward symmetry plane heat flux and temperature for both equilibrium and nonequilibrium flow at 32-deg angle of attack as a function of axial body length.

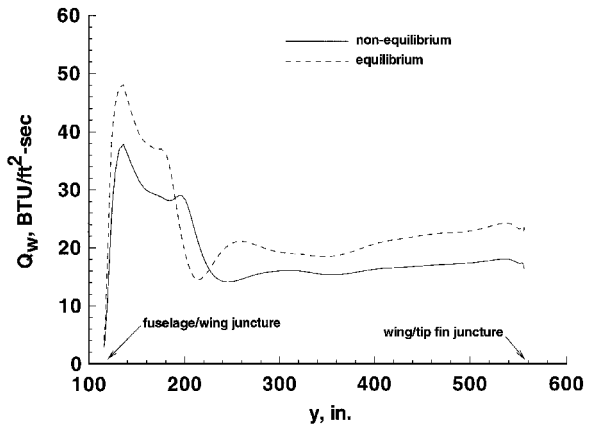

a) Heat flux

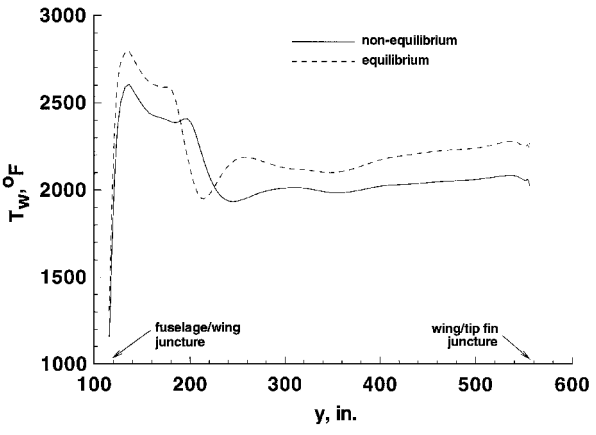

b) Temperature

Fig. 7 Wing leading-edge distribution of surface heat flux and temperature for both equilibrium and nonequilibrium flow at 32-deg angle of attack as a function of distance outboard of the vehicle centerline.

in Figs. 7a and 7b, where the surface thermal properties have been plotted as a function of the distance along the wing leading edge measured from the symmetry plane. Again, for equilibrium flow, the heating rates are substantially higher than those for nonequilibrium flow. The high level of heating near the wing/fuselage juncture is the result of a shock/shock interaction between the forebody bow shock and the wing shock (Fig. 8). As stated in Ref. 16, the two chemistry models produce different shock topologies, which accounts for the different spatial distributions of heating and temperature signatures along the wing leading edge. Across the wing leading edge, the equilibrium flow solution predicts heating rates 20–30% higher than those for the nonequilibrium flow solution. Surface temperatures in the wing/fuselage juncture area exceed or are very near the multiple-use limit for rigid ceramic tiles depending on the chemistry model being considered but are within the limits for RCC/ACC, which are materials typically used for TPS on wing leading edges. Because of the large size of this vehicle, the shear layer resulting from the shock/shock interaction may be transitional or turbulent. Thus, the laminar flow results presented are not a conservative prediction of the thermal environment. Outside of the shock interaction region, the wing leading-edge surface temperatures are within the multiuse limits of ceramic TPS.

The surface thermal environment for the tip fin leading edge is plotted in Figs. 9a and 9b as a function of tip fin height. The first heating pulse around $x = -50$ in. is due to the wing/tip fin juncture. The second heating pulse is due to a shock/shock interaction between the wing shock and the tip fin shock generated when the tip fin protrudes through the wing shock and into the freestream. Again, the dependency of the shock topology on the chemistry model leads to different spatial distributions of heating and temperature along the tip fin leading edge. For the equilibrium case, the multiple-use limit for all of the listed materials is exceeded. The maximum temperature is still less than the single-use limit of RCC/ACC. For the nonequilibrium case, the surface temperatures

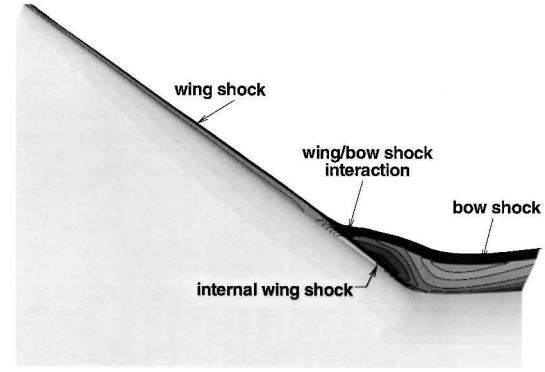

Fig. 8 Shock structure in front of the wing/body juncture; a planform view.

still exceed the multiple-use limits of all of the TPS materials except RCC/ACC.

Angle-of-Attack Analysis

The present nominal angle of attack for the peak heating case being considered is 32 deg, with potential dispersions from this norm expected to be ±4 deg. To quantify the thermal environment at these angle-of-attack bounds, two additional cases were run at $\alpha = 28$ and 36 deg for nonequilibrium flow chemistry. These results are discussed in the following section.

The fuselage windward centerline plot (Fig. 10) shows that the stagnation point heat flux is insensitive to these relatively small changes in angle of attack, which is not unexpected as the surface radius of curvature is nearly constant in the immediate stagnation region. Over the remaining length of the vehicle, there is an angle-of-attack influence on the surface heat flux that is nominally 20%.

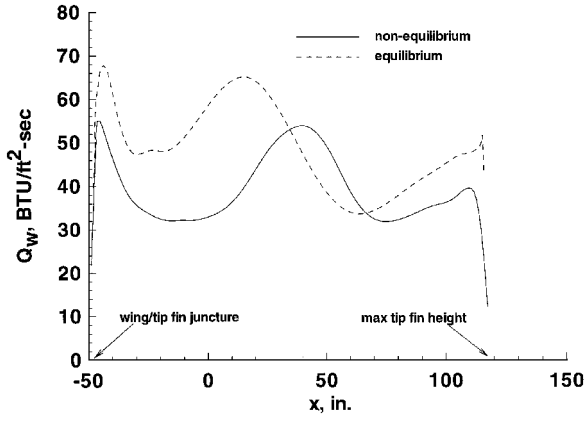

a) Heat flux

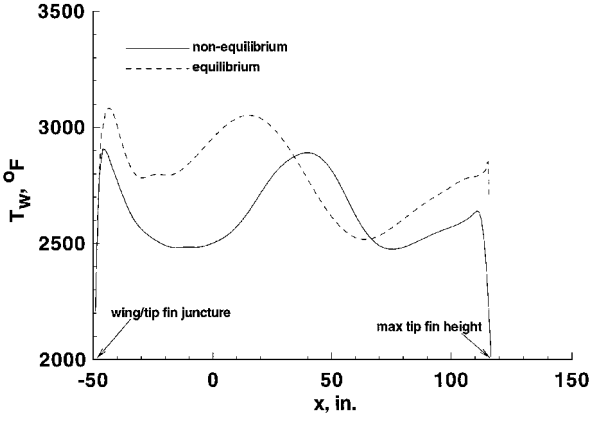

b) Temperature

Fig. 9 Tip fin leading-edge distribution of surface heat flux and temperature for both equilibrium and nonequilibrium flow at 32-deg angle of attack as a function of tip fin height.

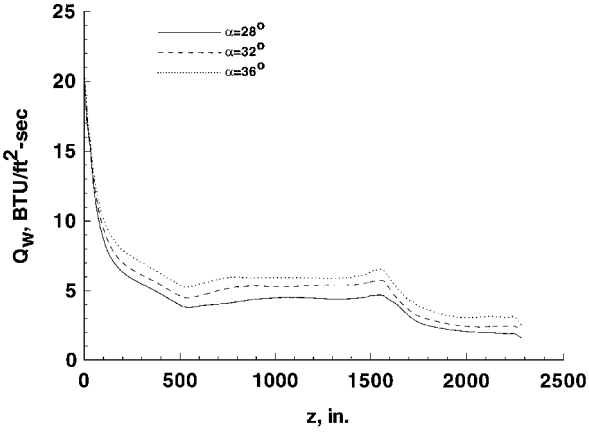

Fig. 10 Windward centerline distribution of surface heat flux for nonequilibrium flow and angles of attack of 28, 32, and 36 deg as a function of vehicle axial length.

On the wing leading edge (Fig. 11), the magnitude of the change in heat flux at the surface with change in angle of attack is similar to that found on the windward centerline. Note, however, that the trend is reversed. On the centerline, the heating increases with increasing angle of attack, whereas the opposite is true on the wing leading edge. This difference is due to two effects. First, as the vehicle rotates down, the angle between the incoming flow and the tangent plane to the surface at the wing leading edge increases; thus, the local surface pressure increases. Second, at the same time, the effective radius of surface curvature seen by the incoming flow decreases. Both of these effects, increasing pressure and decreasing radius of curvature, lead to higher heating.

Unlike the effect on the fuselage windward centerline and wing leading edge, small changes in angle of attack lead to large changes

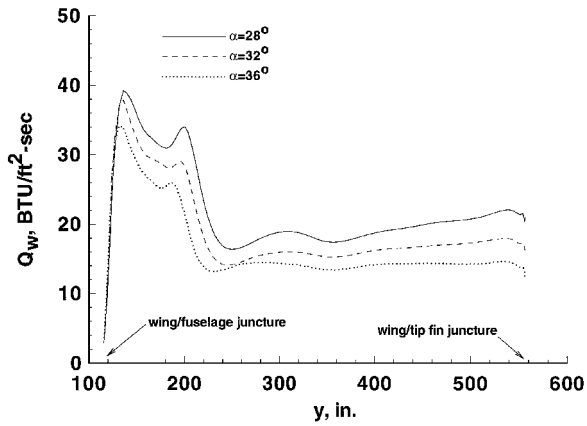

Fig. 11 Wing leading-edge distribution of surface heat flux for nonequilibrium flow and angles of attack of 28, 32, and 36 deg as a function of distance outboard of the vehicle centerline.

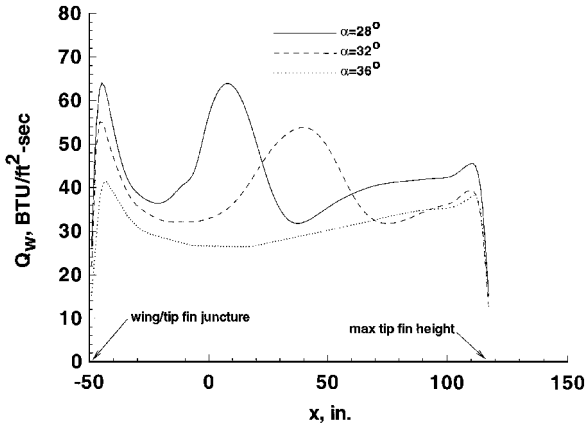

Fig. 12 Tip fin leading-edge distribution of surface heat flux for nonequilibrium flow and angles of attack of 28, 32, and 36 deg as a function of tip fin height.

in the surface heat flux on the tip fin. As shown in Fig. 12, surface heat flux can decrease by as much as 130% for an angle-of-attack change from 28 deg up to 36 deg. As already described, the first heating pulse is due to the wing/tip fin juncture, whereas the second pulse is the result of a shock/shock interaction. In Figs. 13a and 13c, the locations of the wing and tip fin shocks are plotted in a plane that is normal to the surface along the tip fin leading edge. At $\alpha = 28$ deg, approximately 70% of the tip fin is exposed to the freestream and is subjected to the effects of a strong shock interaction, whereas at $\alpha = 36$ deg, the tip fin lies entirely within the wing shock. By exposing the tip fin to the freestream, the potential exists for the surface temperatures to exceed the multiuse limits of RCC/ACC. On the other hand, keeping the tip fin immersed in the wing shock layer reduces the leading-edge surface temperatures to such a level that the multiuse limit for rigid ceramic TPS is not exceeded.

Tip Fin Parameterization

In the results shown to this point, it is clear that maximum surface temperatures occur on the tip fin leading edge. Thus, the tip fin represents the greatest challenge to the TPS designer. The angle-of-attack heating calculations demonstrated that the orientation of the leading edge relative to the oncoming stream had a large effect. In addition, tip fin and wing leading-edge radii will also have a strong influence on surface heating. To investigate these two parameters, additional solutions were obtained for tip fins having leading-edge sweep angles of 24 and 40 deg and leading-edge radii of 1.16 and 2.31 in. on a 32 deg leading-edge tip fin at the nominal flight angle of attack of 32 deg. The leading-edge heat flux for the additional leading-edge sweep angles is presented in Fig. 14 as a function of tip fin height. These solutions show that the relation between tip fin leading-edge sweep and flight-path inclination strongly influences the heating levels on the tip fin leading edge. And, for these

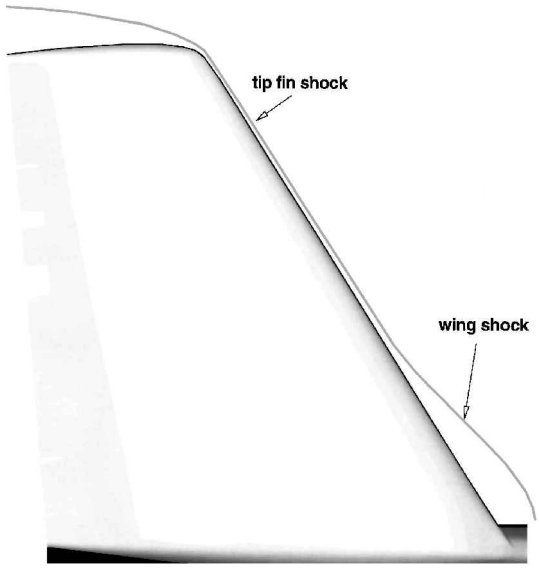

a) α = 28 deg

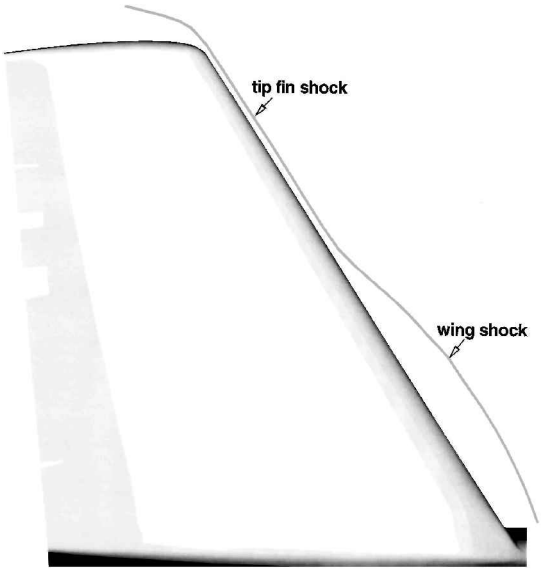

b) α = 32 deg

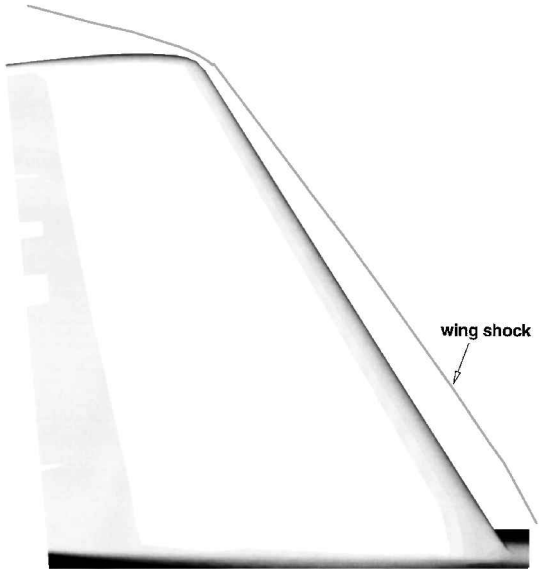

c) α = 36 deg

Fig. 13 Tip fin shock structure in a plane normal to the tip fin leading edge for nonequilibrium flow.

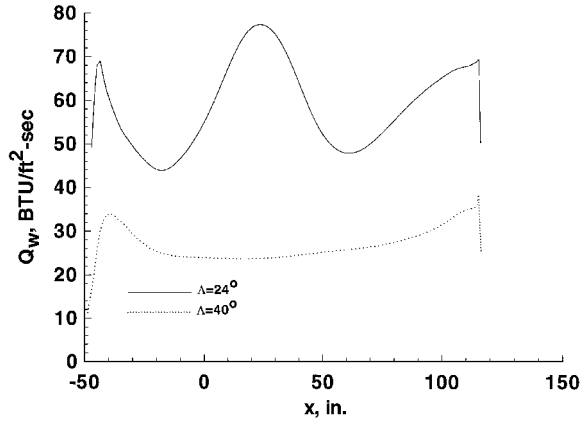

Fig. 14 Tip fin leading-edge distribution of surface heat flux for nonequilibrium flow at 32-deg angle of attack for leading-edge sweep angles of 24 and 40 deg as a function of tip fin height.

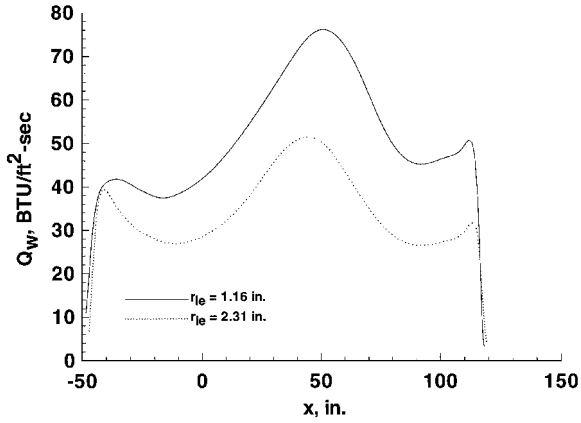

Fig. 15 Tip fin leading-edge distribution of surface heat flux for nonequilibrium flow at 32-deg angle of attack for half-span height leading edge radii of 1.16 and 2.31 in.

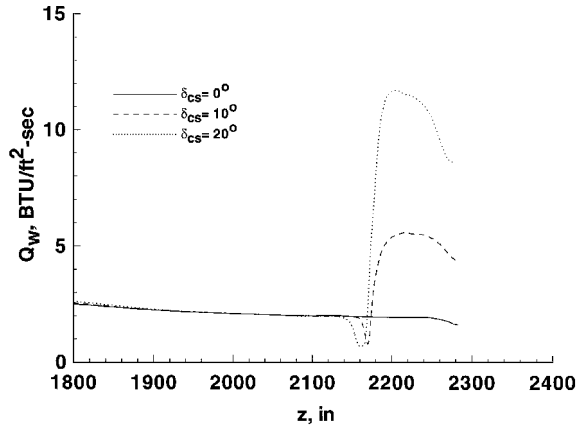

Fig. 16 Centerline distribution of surface heat flux on the deflected control surface for nonequilibrium flow at 28-deg angle of attack and control surface deflections of 0, 10, and 20 deg.

configurations, it means the difference between the application of a multiuse as opposed to a single-use TPS.

The effect of varying leading-edge radius on the tip fin leading heat flux is shown in Fig. 15 as a function of tip fin height. Clearly, the leading-edge radius has as large an impact on the leading-edge heating as does the leading-edge sweep angle. The maximum heating levels for the $\Lambda = 24$ deg case and the $r_{le} = 1.16$ in. case are nearly the same, and both cases correspond to the surface temperatures that are near the single-use limit for RCC/ACC.

The analysis was carried out at the peak stagnation-point heating point on the vehicle's re-entry trajectory. As shown, the maximum heating does not occur at the stagnation point but on the tip fin leading edge. There is no reason to believe that the maximum

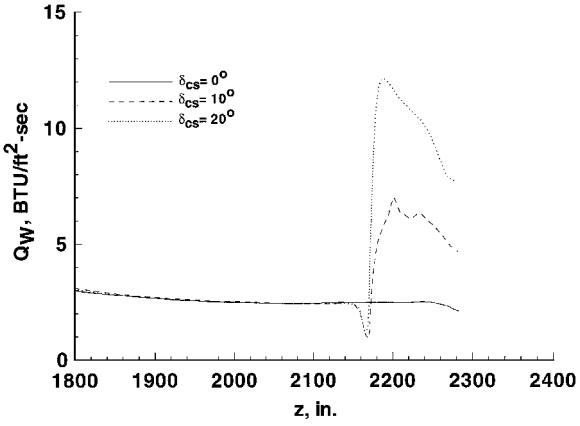

Fig. 17 Centerline distribution of surface heat flux on the deflected control surface for nonequilibrium flow at 32-deg angle of attack and control surface deflections of 0, 10, and 20 deg.

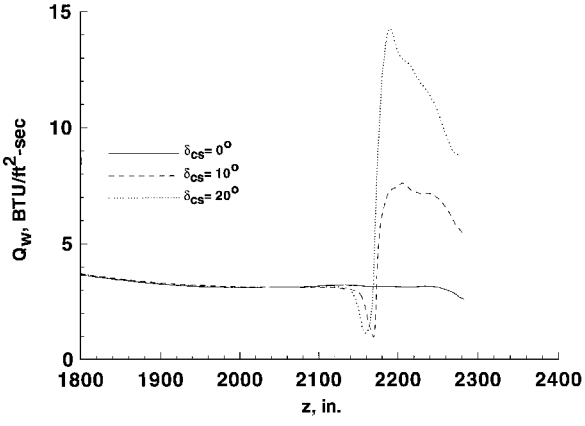

Fig. 18 Centerline distribution of surface heat flux on the deflected control surface for nonequilibrium flow at 36-deg angle of attack and control surface deflections of 0, 10, and 20 deg.

heating on the tip fin occurs at this condition, and several other points on the trajectory need to be checked to establish the maximum heating at this point on the vehicle. Given the strong influence of tip fin geometry on tip fin leading-edge heating demonstrated, it may be possible to tailor the geometry of the tip fin to minimize the temperatures on the tip fin leading edge.

Control Surfaces

At hypersonic speeds, the control surfaces, body flap and elevons, are assumed to deflect in unison, as shown in Fig. 1. In the following discussion, analysis of the thermal environment of the deflected control surfaces is based on the nonequilibrium flow model.

The centerline surface heat fluxes for control-surface deflections of 0, 10, and 20 deg at angles of attack of 28, 32, and 36 deg are shown in Figs. 16–18. For the highest heating case at each angle of attack, $\delta_{cs} = 20$ deg, the corresponding temperature levels are well within the multiuse limits of rigid ceramic TPS. In Ref. 16 it was shown that, as configured, the vehicle would trim at this peak heating condition at a δ_{cs} from 7.5 to 10 deg for the present angle-of-attack range. At these deflection angles, on the centerline, the control surface will only see maximum temperatures in the 1500–1600°F range. A surface temperature map for the entire control surface for the $\alpha = 32$ deg and $\delta_{cs} = 20$ deg condition is shown in Fig. 19, and the corresponding surface streamline pattern is shown in Fig. 20.

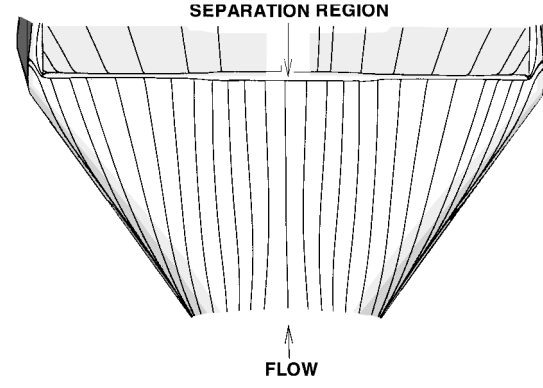

Fig. 20 Surface streamline patterns for nonequilibrium flow at 32-deg angle of attack and a control surface deflection of 20 deg.

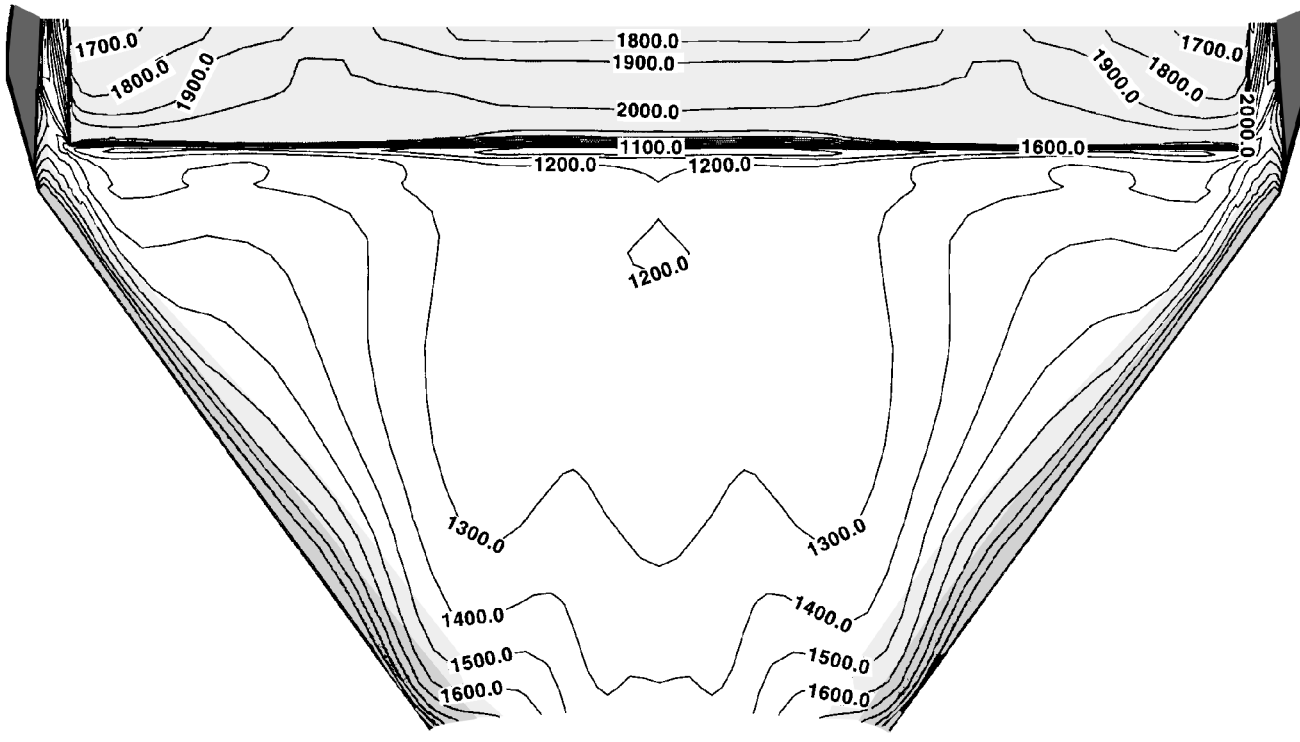

Fig. 19 Windward surfaces temperature contours (°F) for nonequilibrium flow at 32-deg angle of attack and a control surface deflection of 20 deg.

Figures 19 and 20 show only a small separation region in front of the control surfaces, which is consistent with the results presented in Ref. 3 for flow over the Shuttle Orbiter control surfaces. There is only a 300°F temperature variation over the entire control surface area. The patterns shown are typical of those found for all angles of attack and control surface deflections.

Concluding Remarks

The predicted surface thermal environment for a representative SSTO winged body vehicle at the peak heating point, $M_\infty = 21.89$ and $h = 233{,}000$ ft, on a nominal re-entry trajectory has been presented. Surface maps of heating and temperature for the baseline configuration for both equilibrium and nonequilibrium flow show that, for the nominal angle of attack and ±4-deg increments, the majority of the vehicle surface is subject to a moderate thermal environment due to the large size of the vehicle, with surface temperatures that fall well within the multiuse limits of numerous TPS materials. This analysis identified the nose stagnation region, the wing/fuselage juncture, the wing leading edge, and the tip fin leading edge as areas of high heating on the vehicle. Of these four areas, only temperatures on the tip fin leading edge are high enough to present a serious TPS materials problem. Parametric studies of tip fin leading-edge sweep and leading-edge radius effects show that both have a strong influence on the thermal environment of the tip fin leading edge. The thermal environment of the control surfaces (combined body flap and elevons) was investigated for control surface deflections up to 20 deg. For all of the control surface configurations, the surface temperatures fell below the multiuse temperature limits for all rigid, nonmetallic TPS materials. And, for the most severe case, the temperature variation over the surfaces was less than 300°F.

References

[1]"Access to Space Study—Summary Report, Office of Space Systems Development," Office of Space and Systems Development, NASA Headquarters, Jan. 1994.

[2]Freeman, D. C., Talay, T. A., Stanley, D. O., Lepsch, R. A., and Wilhite, A. W., "Design Options for Advanced Manned Launch Systems," *Journal of Spacecraft and Rockets*, Vol. 32, No. 2, 1995, pp. 241–249.

[3]Gnoffo, P. A., Weilmuenster, K. J., and Alter, S. J.,"Multiblock Analysis for Shuttle Orbiter Re-Entry Heating from Mach 24 to Mach 12," *Journal of Spacecraft and Rockets*, Vol. 31, No. 3, 1994, pp. 367–377.

[4]Steinbrenner, J., Chawner, J., and Pouts, C., "Multiple Block Grid Generation in the Interactive Environment," AIAA Paper 90-1602, June 1990.

[5]Alter, S. J., and Weilmuenster, K. J., "The Three-Dimensional Multi-Block Advanced Grid Generation System (3DMAGGS)," NASA TM-108985, May 1993.

[6]Weilmuenster, K. J., and Gnoffo, P. A., "Solution Strategy for Three-Dimensional Configurations at Hypersonic Speeds," *Journal of Spacecraft and Rockets*, Vol. 30, No. 4, 1993, pp. 385–394.

[7]Gnoffo, P. A., Gupta, R. N., and Shinn, J., "Conservation Equations and Physical Models for Hypersonic Air Flows in Thermal and Chemical Nonequilibrium," NASA TP-2867, Feb. 1989.

[8]Gnoffo, P. A., "Upwind-Biased, Point-Implicit Relaxation Strategies for Viscous Hypersonic Flows," AIAA Paper 89-1972, June 1989.

[9]Gnoffo, P. A., "An Upwind Point Implicit Relaxation Algorithm for Viscous Compressible Perfect-Gas Glows," NASA TP-2953, Feb. 1990.

[10]Roe, P. L., "Approximate Riemann Solvers, Parameter Vectors, and Difference Schemes," *Journal of Computational Physics*, Vol. 43, Oct. 1981, pp. 357–372.

[11]Harten, A., "High Resolution Schemes for Hyperbolic Conservation Laws," *Journal of Computational Physics*, Vol. 49, No. 3, 1983, pp. 357–393.

[12]Yee, H. C., "On Symmetric and Upwind TVD Schemes," NASA TM-86842, Sept. 1985.

[13]Srinivasan, S., Tannehill, J. C., and Weilmuenster, K. J., "Simplified Curve Fits for the Thermodynamic Properties of Equilibrium Air," NASA RP-1181, Aug. 1987.

[14]Thompson, R. A., "Comparison of Nonequilibrium Viscous-Shock-Layer Solutions with Shuttle Heating Measurements," *Journal of Thermophysics and Heat Transfer*, Vol. 4, No. 2, 1990, pp. 162–169.

[15]Goldstein, H., "Reusable Thermal Projection System Development—A Perspective," NASA CP-3157, Feb. 1992.

[16]Weilmuenster, K. J., Gnoffo, P. A., Greene, F. A., Riley, C. J., Hamilton, H. H., II, and Alter, S. J., "Hypersonic Aerodynamic Characteristics of a Proposed Single-Stage-to-Orbit Vehicle," *Journal of Spacecraft and Rockets*, Vol. 33, No. 4, 1996, pp. 463–469.

B. A. Bhutta
Associate Editor